European Journal of Engineering and Applied Sciences

ISSN: 2651-3412 (Print) & 2667-8454 (Online)
Journal homepage: http://dergipark.gov.tr/EJEAS
Published by Çorlu Faculty of Engineering, Tekirdağ Namık Kemal University

European J. Eng. App. Sci. 4(2), 66-89, 2021

Research Article

The 30 October 2020, M_w 6.6 Sisam (Samos) Earthquake: Interpretation of Strong Ground Motions and Post-Earthquake Condition of Nearby Structures

Vesile Hatun Akansel[1], Gülen Özkula[2,*]

[1] Department of Civil Engineering, Muğla Sıtkı Koçman University, Muğla, Turkey
[2] Department of Civil Engineering, Tekirdağ Namık Kemal University, Tekirdağ, Turkey

Received: 13.12.2021 Accepted: 24.12.2021

Abstract: A major magnitude M_w 6.6 earthquake struck offshore of the city of İzmir, Turkey and the city of Neon Karlovasion, Greece which has the epicenter located at north of Sisam/ Samos Island in the eastern Agean Sea on October 30th, 2020. The moment magnitude of the earthquake has been reported variously, such as 6.6, 6.9 and 7.0 by different agencies. Seismic instruments indicate the earthquake originated at a depth of 17.2 and 21 kilometers according to the Disaster and Emergency Management Presidency (AFAD) of Turkey and USGS. Doğanbey Payamlı, Ürkmez, Gümüldür, Kavakdere are the closest coastal villages of İzmir to the epicenter. The earthquake affected the mid-rise buildings located on the soft soil and then, tsunami stroked the coastal villages of İzmir. In this study, the strong ground motion records in a distance range from epicenter to 150 km are analyzed to investigate the characteristic of the ground motions. The post-earthquake field observations mainly for the mid-rise reinforced concrete structures are reported. The spatial distribution of the damage indicates a basin effect within the Bayraklı, Bornova and Karşıkaya regions. The 8-10 story mid-rise buildings affected from the main and aftershocks and the north coasts of İzmir affected from the tsunami were the main observations of this earthquake.

Keywords: Samos earthquake, strong ground motion records, GMMs, damage distribution

30. Ekim. 2020, M_w 6.6 Samos Depremi Kuvvetli Yer Hareketlerinin Yorumlanması ve Yakındaki Yapıların Deprem Sonrası Durumu

Özet: 30 Ekim 2020'de Ege denizi açıklarında, merkez üssü Sisam/Samos Adası'nın kuzeyinde bulunan Yunanistan'ın Neon Karlovasion kentinin açıklarında 6.6 büyüklüğünde bir deprem meydana gelmiştir. Deprem farklı kurumlar tarafından 6.6, 6.9 ve 7.0 gibi çeşitli şekillerde rapor edilmiştir. Bu çalışmada, yer hareketlerinin özelliklerini araştırmak için merkez üssünden 150 km'ye kadar olan bir mesafedeki kuvvetli yer hareketi kayıtları analiz edilmiştir. Deprem sonrası saha gözlemleri ağırlıklı olarak orta yükseklikteki betonarme yapılar için rapor edilmiştir. Hasarın mekansal dağılımı Bayraklı, Bornova ve Karşıkaya bölgelerinde bir havza etkisine işaret etmektedir. Ana ve artçı sarsıntılardan etkilenen 8-10 katlı orta katlı binalar ve tsunamiden etkilenen İzmir'in kuzey kıyıları bu depremin başlıca gözlemleridir.

Anahtar Kelimeler: *Samos depremi, deprem kayitlari, GMMs, .hasar dağılımı*

[*] Corresponding author.
E-mail address: gozkula@nku.edu.tr (G. Ozkula)

1. Introduction

İzmir is located on the west coasts of Turkey which is close to Greek islands such as Sakız, Midilli and Sisam (Samos). The 30 October 2020 Sisam earthquake affected Sisam Island, İzmir and its districts. Doğanbey Payamlı, Ürkmez, Gümüldür, Kavakdere are the closest coastal villages of İzmir to the epicenter. The fault rupture lowered the seafloor and a tsunami which stroked the Sığacık Bay and Akarca on the north, Alaçatı and Zeytineli on the northwest and Tepecik and Gümüldür on the northeast of İzmir, occurred. Samos Island and the coast of Seferihisar Bay were affected the most from the tsunami. According to the GEER (2020) the maximum runup and inundation lengths of about 3.8 m and 2500 m measured in Akarca and along the Alacati Azmak stream, respectively, resulting in substantial property losses. The mid-rise buildings located on the soft soil conditions are affected from the main and aftershocks in İzmir, especially, in Bayraklı region.

The districts of Karsiyaka and Cigli are located on a typical alluvial delta in front of the Yamanlar mountain blocks. The ancient Gediz River Delta, located in the northwestern part of the Karsiyaka and Bostanl districts, was formed by sedimentation of alluvial deposits carried by the Gediz River in the Quaternary [Cetin et al. (2020)].Bayrakli, the district hardest hit by the earthquake, lies on a very deep water basin, which is bordered by hills to the north and south. While most of the district is founded on Quaternary alluvial sediments of the basin, the peripheral areas extend over the rising slopes of the rock outcrop to the north and south. The detailed geological and geophysical investigations in the district of Bayrakl showed the subterranean soil and rock properties in the alluvial basin by Pamuk et al (2017,2018,2019).The marcoseismic intensity, shakemap is given in Figure 1. The AFAD named the event such as Seferihisar (İzmir) earthquake with magnitude of 6.6. The latitude and longitude of the epicenter are given as 37.879 and 26.703, respectively by AFAD. The depth is 14.9 km. The closest distance to the epicenter is 17.26 km which is Seferihisar, İzmir on the coast of Turkey. According to the AFAD, the focal mechanism of the earthquake is 95º strike, 43º dip and -87º rake angle (Havskov and Ottemoller (1999)). There is a discrepancy in the solution of the event by USGS and AFAD. USGS named the event as Néon Karlovásion, Greece with magnitude of 7.0, 21.0 km depth, latitude of 37.913 and longitude of 26.779. The focal mechanism of the event is reported by USGS as is 93º strike, 61º dip and -91º rake angle. This discrepancy may affect and result in differences in the Ground Motion Models (GMM) calculations. Greek strong motion network Institute of Engineering Seismology and Earthquake Eangineering (ITSAK) and National Observatory of Athens (NOA) announced the event with magnitude of 6.9.

Figure 1. Macroseismic intensity, ShakeMap (Adapted from AFAD webpage (AFAD ,2020)]

The main shock affected the masonry structures in the near fault region such as the masonry building located on Sisam Island and mid-height buildings located in İzmir and districts. The Bayraklı district is the most affected region from the main and aftershocks. The maximum recorded peak ground acceleration (PGA) value of the event at Sisam was 0.23g and this is expected design level earthquake for Sisam, however, recorded PGA values were below the expected design level on rock site of the Aegean coasts of Turkey. The damaged buildings are mostly located on the soft soil type. The Turkish Republic of Ministry of Environment and Urbanization employed over 600 team to assess the buildings in the affected area and 54 collapsed, 36 demolished urgently, 602 heavily damaged, 720 moderately damaged, 6848 slightly damaged and 136.913 no-damaged structures. As a direct result of this earthquake, 116 lives were lost and over 1030 people were injured. In this study, the main scope is to investigate the recorded ground motions and to assess the globally and locally developed ground motion prediction models together for their performance; to compare measured intensities with the code-specified spectra; to investigate the reasons of damaged building distribution after the main shock and aftershocks and to assess the common failure types in the building stock.

1.1. Seismicity of the Region and Historical Earthquakes

The northern Sisam fault which is the source of the 30 October 2020 Sisam earthquake, located on the highly deformed back-arc area in the middle-eastern part of the Aegean microplate. The subduction of the Eastern Mediterranean oceanic plate under the Aegean microplate and the westward movement of the Anatolian micro plate along the North Anatolian Fault Zone provide the formation of regional deformation. The Aegean microplate moves almost uniformly towards the South-South-West (SSW) at a speed of approximately 33 mm / year [DAUM (2020)]. The rupture as occurring on a fault dipping 40-45^{o} to the north, with an along-strike length of 32-38 km and down-dip width of 15 km given in GEER (2020) report and the similar results are reported by Tan et al. (2014). The active faults in the region are adapted from the GEER (2020) report as given in **Figure 2**. The details of the faults in the region are not in the scope of this study and the readers are encouraged to read the DAUM (2020) report for fault details. In this study, only the active faults existing on the Sisam Island will be introduced. The main and aftershocks showed that the rupture was

concentrated on the North Sisam Fault, which is about E-W trending normal fault character. Some of the aftershocks occurred near the junction points of the extensions of the Karliova Fault and Tuzla Fault in the sea.

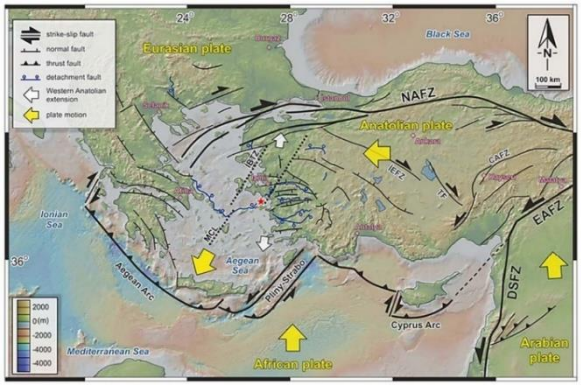

Figure 2. Active Faults in the region (Adapted from GEER (2020))

The earthquakes with 5.5 ≤ M ≤ 7.0 magnitude recorded events by AFAD in and surrounding of İzmir since 1975 are given in **Table 1**. The maximum magnitude is recorded as 6.6 by AFAD for the 30 October 2020 Sisam Earthquake. **Figure 3** also shows the earthquakes with M>3 and the earthquakes listed in **Table 1**.

The seismicity of the region dates to 200 BC. Twelve historical earthquakes with a magnitude of VII and above in this region are listed. as; 200 BC- M6.3-VIII, 47 BC – M6.9 – VIII, 17.06.1751-M6.9-VIII, 03.04.1831- M6.0-VII, 13.06.1846-M6.0-VII, 11.10.1865-M6.0-VII, 16.05.1868-M6.0-VII, 31.01.1873-M6.5-VII, 14.10.1877-M6.0-VIII, 14.12.1890-M6.2-VIII, 12.03.1893-M6.6-VII and 11.08.1904-M6.8-VIII (Ambraseys 2009; Tan et al. 2014).

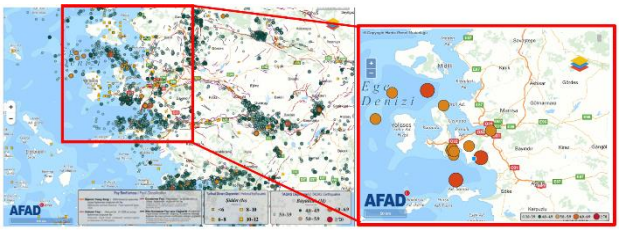

Figure 3. Quaternary faults and epicenters of earthquakes in the region surrounding İzmir. (adapted from tadas.afad.gov.tr). Left: Regional Turkish accelerometric database and earthquakes with M ≥ 3.0 since 1975. Right: Earthquakes since 1975 with 5.5 ≤ M ≤ 7.0.

2. Measured Strong Ground Motion Records

The 30 October 2020 Sisam earthquake has been recorded in different stations. AFAD stations located in 150 km distance

Table 1. The eartquakes with 5.5 ≤ M ≤ 7.0 magnitude in and around İzmir since 1975 (tadas.afad.gov.tr) (AFAD (2020,c))

	Event	Epicenter						
EventID	Date	Agency	Lon.	Lat.	Type	Magnitude	Depth	Location
483762	30-10-2020	AFAD	26.7030	37.8790	M	6.6	14.9	(Sisam) (Aegean Sea)
375576	12-06-2017	AFAD	26.3126	38.8488	M	6.2	15.86	Karaburun (İzmir)
263786	20-10-2005	GDDA	26.6708	38.1535	M	5.8	15.4	-/-/Turkey
264639	17-10-2005	GDDA	26.6406	38.2048	MD	5.5	11.0	Urla (İzmir)
253004	17-10-2005	GDDA	26.6586	38.2202	M	5.8	18.6	Urla (İzmir)
252972	17-10-2005	GDDA	26.6770	38.1921	M	5.5	20.5	-/-/Turkey
236780	10-04-2003	ISC	26.8895	38.2466	M	5.7	11.3	Urla (İzmir)
243329	10-06-2001	ISC	25.5930	38.5410	M	5.6	32.0	Aegean Sea (-)
	14-11-1997	ISC	25.8212	38.8243	M	5.8	2.3	
	20-07-1996	GDDA	27.0500	38.1200	M	6.1		
243796	24-05-1994	ISC	26.5335	38.6863	M	5.5	10.0	-/-/Turkey
247417	06-11-1992	ISC	26.9560	38.1091	M	6.0	17.2	Menderes (İzmir)
	16-12-1977	ISC	27.1882	38.4140	M	5.6	24.2	

to the epicenter of the event are selected for this report and the records are listed in **Table 2**. Only the first station, in the **Table 2,** is obtainded from the Greek strong motion network ITSAK. Average seismic shear-wave velocity for the surface to a depth of 30 meters, V_{S30} values of these records were given in the **Table 2** except for the last eight stations. PGA values of three components, R_{jb}, R_{rup}, R_{epi}, R_{hyp} distances and soil classes are also given in **Table 2**. Sisam, Kuşadası, Menderes, Karşıyaka Orman İşletme (Karşıyaka - Forest Management Department), Bayraklı, Bayraklı Teknik Lise (Bayraklı- Technical High School) and Çeşme stations are investigated in detail. The station names are in Turkish in the AFAD database and therefore in the text, they were refered as what they are. In **Figure 4**, the soil classes of each station studied in this report are given with different colors. The enlarged part of the **Figure 4,** is showing the stations located in Bayraklı district which is highly affected from the earthquake. There exists four soil class type varying from ZB to ZE.

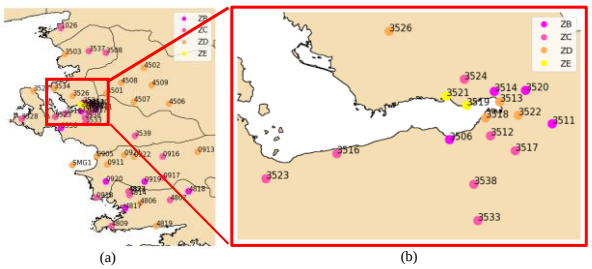

Figure 4. a) Strong ground motion stations within 150 km from the epicenter of the Sisam Earthquake; numbers indicate station codes according to AFAD b) İzmir, closer stations

with focus on the Bayraklı district

The selected stations from **Table 2** with the soil class and R_{jb} distances are depicted in **Figure 5.** These stations are showing higher PGA vaues. The highest PGA recorded for this event is 0.23 g at SMG1 (Sisam) station which has soil class ZD. And is the closest station to the epicenter. The duration of strong motion is varying at each station and also the frequency content is changing depending on the soil class and attanuation

3. Ground Motion Production Models

All stations excluding the Sisam (SMG1) given in **Table 2** are investigated in detail to assess the ground motion prediction models which are plenty in literature dating back to 1964. Douglas (2019) reported 452 ground motion prediction equations in his report. Some of these models are global while the others were developed for regional predictions. Ulusay et al. (2004); Kalkan and Gülkan (2004), and KAAH (2015) are few of them derived for Turkey while PEER using the global datasets such as NGA-1 and NGA-2 [Bozorgnia et al. (2014)] are the example for global models.The ground motion prediction models are developed by using the ground motion database and derivation basics of the ground motion prediction equations are given in detail by Boore et al. (1997)

Table 2. Strong motion stations (tadas.afad.gov.tr, ITSAK-EPPO Network (AFAD (2020,c), ITSAK (2020a), NOA (2020))

Station Code	Name	V_{S30} (m/s)	Latitude	Longitude	PGA_NS (cm/s^2)	PGA_EW (cm/s^2)	PGA_UD (cm/s^2)	R_{jb} (km)	R_{rup} (km)	R_{epi} (km)	R_{hyp} (km)	Soil Class	S_s	S_1	M_w
SMG1	Sisam/Samos*	380	37.7	26.84	158	227	134	13	18	23	26	ZD	-	-	6.9
0905	Kuşadası*	369	37.86	27.27	179	144	80	36	41	43	46	ZD	1.1	0.3	6.6
911	Söke	307	37.76	27.39	48	67	47	48	53	56	58	ZD	1.3	0.3	6.6
0913	Aydın-Kuyucak	301	37.91	28.47	7.5	11	4.2	141	142	148	149	ZD	1.4	0.3	6.6
0916	Aydın-Köşk	371	37.86	28.05	9.8	15	7.4	104	106	112	113	ZC	1.4	0.4	6.6
0917	Çine	580	37.61	28.06	13	13	8.6	110	111	117	118	ZC	0.8	0.2	6.6
0918	Didim	630	37.37	27.26	38	31	21	64	68	72	74	ZC	0.8	0.2	6.6
0919	Karpuzlu	986	37.56	27.84	21	18	15	93	95	100	101	ZB	0.8	0.2	6.6
0920	Söke-2	894	37.56	27.37	26	31	22	57	60	64	66	ZB	1.0	0.2	6.6
3503	Dikili	193	39.07	26.89	56	45	17	125	127	132	133	ZD	1.0	0.2	6.6
3506	Konak	771	38.39	27.08	44	41	24	55	59	62	64	ZB	1.1	0.3	6.6
3508	Kınık	558	39.09	27.37	14	17	7.5	136	137	143	144	ZC	1.0	0.2	6.6
3511	Bornova-Enko	827	38.42	27.26	29	41	19	65	68	73	74	ZB	1.1	0.3	6.6
3512	Buca	468	38.4	27.15	58	57	28	58	62	66	68	ZC	1.1	0.3	6.6
3513	Bayraklı*	195	38.46	27.17	106	95	44	65	68	72	74	ZD	1.1	0.3	6.6
3514	Bayraklı-Teknik Lise*	836	38.48	27.16	39	56	25	66	69	73	75	ZB	1.1	0.3	6.6
3516	Güzelbahçe	460	38.37	26.89	47	48	32	47	51	55	57	ZC	1.1	0.3	6.6
3517	Buca-Dokuz Eylül	695	38.38	27.19	40	36	20	58	61	65	67	ZC	1.1	0.3	6.6
3518	Konak-Kültürpark	301	38.43	27.14	106	91	31	61	64	68	70	ZD	1.1	0.3	6.6
3519	Karşıyaka-Orman İşletme*	131	38.45	27.11	150	110	34	62	65	69	71	ZE	1.1	0.3	6.6
3520	Bornova-İstasyon	875	38.48	27.21	36	59	19	68	71	76	78	ZB	1.1	0.3	6.6
3521	Karşıyaka	145	38.47	27.08	111	94	40	62	66	70	72	ZE	1.1	0.3	6.6
3522	Bornova	249	38.44	27.2	74	64	25	64	67	71	73	ZD	1.1	0.3	6.6
3523	Urla	414	38.33	26.77	80	64	37	42	46	49	52	ZC	1.1	0.3	6.6
3524	Karşıyaka-2	459	38.5	27.11	65	68	30	66	69	74	75	ZC	1.1	0.3	6.6
3526	Menemen	205	38.58	26.98	89	82	29	71	74	79	80	ZD	1.0	0.2	6.6
3527	Karaburun	207	38.64	26.51	81	57	47	79	82	87	88	ZD	1.1	0.3	6.6
3528	Çeşme*	532	38.3	26.37	118	149	77	51	55	58	61	ZC	1.0	0.2	6.6
3533	Menderes*	415	38.26	27.13	74	46	37	44	49	51	54	ZC	1.0	0.3	6.6
3534	Foça	327	38.66	26.76	73	92	38	79	81	86	88	ZD	1.1	0.3	6.6
3536	Seferihisar	1141	38.2	26.84	50	79	31	27	34	35	38	ZB	1.1	0.3	6.6
3537	Bergama	608	39.11	27.17	7.5	7.8	7.1	133	134	140	141	ZC	1.1	0.2	6.6
4501	Manisa-Yunusemre	340	38.61	27.38	35	40	24	89	91	96	98	ZD	1.2	0.3	6.6
4502	Akhisar	292	38.91	27.82	23	29	12	138	140	146	147	ZD	1.0	0.2	6.6
4506	Salihli	273	38.48	28.12	24	22	22	128	129	135	136	ZD	1.1	0.3	6.6
4507	Turgutlu	341	38.51	27.71	27	34	19	99	101	106	108	ZD	1.2	0.3	6.6
4508	Saruhanlı	229	38.73	27.56	35	39	16	109	110	116	117	ZD	1.0	0.2	6.6
4806	Milas-3	323	37.3	27.78	23	26	7.4	102	104	110	111	ZD	0.9	0.2	6.6

Table 2. (Cont.) Strong motion stations (tadas.afad.gov.tr, ITSAK-EPPO Network (AFAD (2020,c), ITSAK (2020a), NOA (2020))

Station Code	Name	V_{S30} (m/s)	Latitude	Longitude	PGA_NS (cm/s^2)	PGA_EW (cm/s^2)	PGA_UD (cm/s^2)	R_{jb} (km)	R_{rup} (km)	R_{epi} (km)	R_{hyp} (km)	Soil Class	S_s	S_1	M_w
4807	Yatağan	696	37.34	28.14	8.3	4.3	3.5	127	129	134	135	ZC	0.8	0.2	6.6
4809	Bodrum	747	37.03	27.44	8.2	9.3	6.6	104	106	112	113	ZC	1.0	0.2	6.6
4814	Milas-2	694	37.4	27.66	25	23	10	87	90	95	96	ZC	0.8	0.2	6.6
4817	Milas-4	948	37.24	27.6	16	14	7.6	95	97	102	104	ZB	0.9	0.2	6.6
4818	Kavakdere	1080	37.44	28.36	6.9	3.9	3.4	140	142	148	149	ZB	0.7	0.2	6.6
4819	Milas-5	219	37.03	27.97	16	15	7.4	135	136	142	143	ZD	1.1	0.3	6.6
1026	Balıkesir-Gömeç	-	39.38	26.84	24	31	9.1	159	160	166	167	-	1.0	0.2	6.6
3538	Gaziemir	-	38.32	27.12	85	77	39	49	53	57	59	-	1.1	0.3	6.6
3539	Tire	-	38.1	27.72	38	27	22	79	81	86	88	-	0.8	0.2	6.6
4822	Milas	-	37.44	27.65	33	80	38	84	86	91	93	-	0.8	0.2	6.6
4823	Milas-6	-	37.44	27.64	23	26	19	84	86	91	93	-	0.8	0.2	6.6
921	Germencik	-	37.87	27.59	55	71	23	64	67	72	73	-	1.3	0.3	6.6
922	İncirliova	-	37.85	27.71	60	59	56	74	77	82	83	-	1.4	0.3	6.6
4509	Gölmarmara	-	38.71	27.92	9.1	10	5.8	128	129	135	136	-	1.0	0.2	6.6

* Stations whose records have been used for further processing.

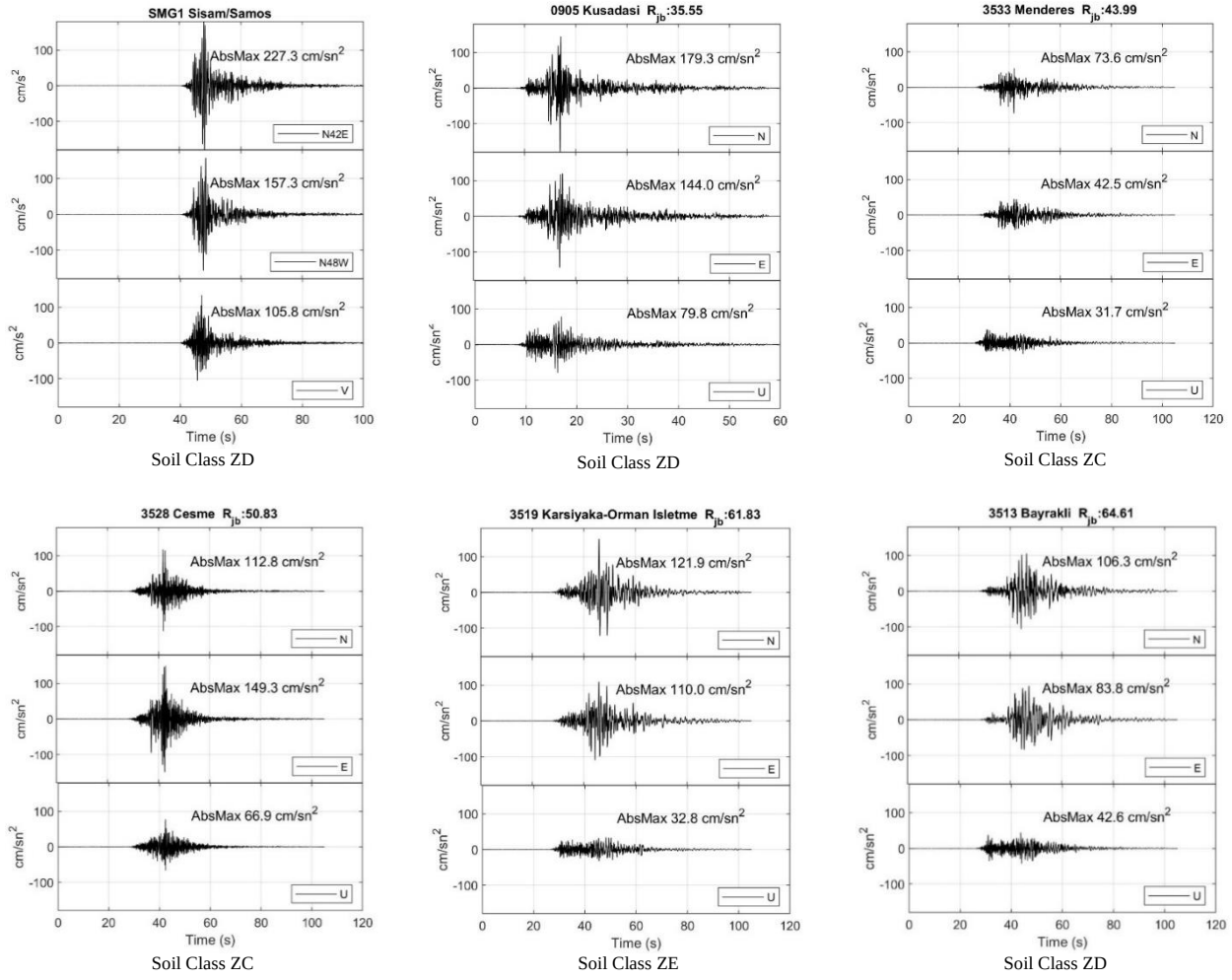

Figure 5. Ground motion records at selected stations (Rjb = Joyner-Boore distance; N: North-South; E: East-West; U: Up-down).

The KG2004 (Kalkan and Gülkan (2004)) ground motion model uses same methodology with Boore et al. (1997) to derive the ground motion model using magnitude, distance and V_{S30} parameters. BSSA2014 (Boore et al. (2014)) is a NGA West-2 model and uses the same parameters as KG2004 and additionally asking for fault type (which has the options of unspecified, strike-slip, normal and reverse), region (which has the options of Global, California, Japan, China / Turkey and Italy), z_1 which is the basin depth defined as 1 km/s shear-wave velocity horizon to the ground surface (which has an option also for unknown z_1 value). The faulting type is chosen as normal; the region is selected as China/ Turkey and z_1 is selected as unknown for BSSA2014 model.

In KAAH2015 ground motion model uses the parameters as; moment magnitude, distance, V_{S30}, style of faulting (which has options of normal, reverse and strike-slip), and the region (which has options of Turkey and Iran). The faulting type is chosen as normal; and the region is selected as Turkey for KAAH2015 ground motion model.

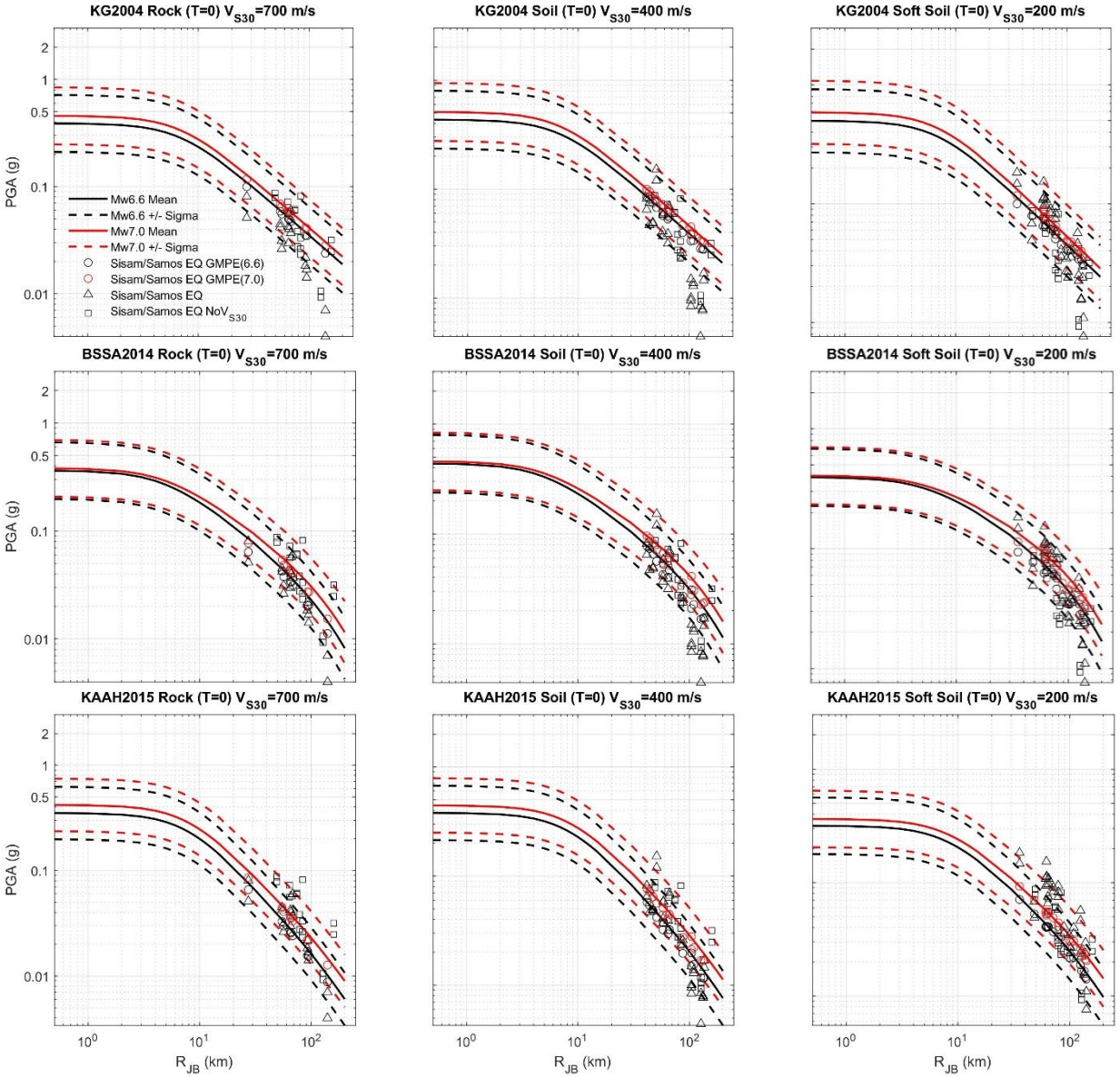

Figure 6. PGA predictions vs measurements among three GMMs

In this study, BSSA 2014 (Boore et al. (2014)) is utilized from the NGA2-West as a global model and KG 2004 (Kalkan and Gülkan (2004)) and KAAH 2015 (Kale et al. (2015)) ground motion prediction models are selected as regional models specifically derived for Turkey and surroundings. These ground motion prediction models are selected to compare the local and global models to see the attenuation. The BSSA 2014 is a global model developed in the NGA West 2 project. The local models, such as, KG 2004 and KAAH 2015 are developed using the Turkish data. The ground motion prediction models are plotted for three different soil type such as soft soil, soil and rock according to the assumed V_{S30} values of 200.0 m/s, 400.0 m/s and 700.0 m/s, respectively. The announced magnitude of the event is showing differences by agencies and this may result in discrepancy therefore, magnitude of 6.6 and 7.0 are both investigated in this study. The stations given in **Table 2** which has no V_{S30} values are included on each soil type according to the assumed V_{S30} values as described. The comparisons are given from **Figure 6** to **Figure 8**. The

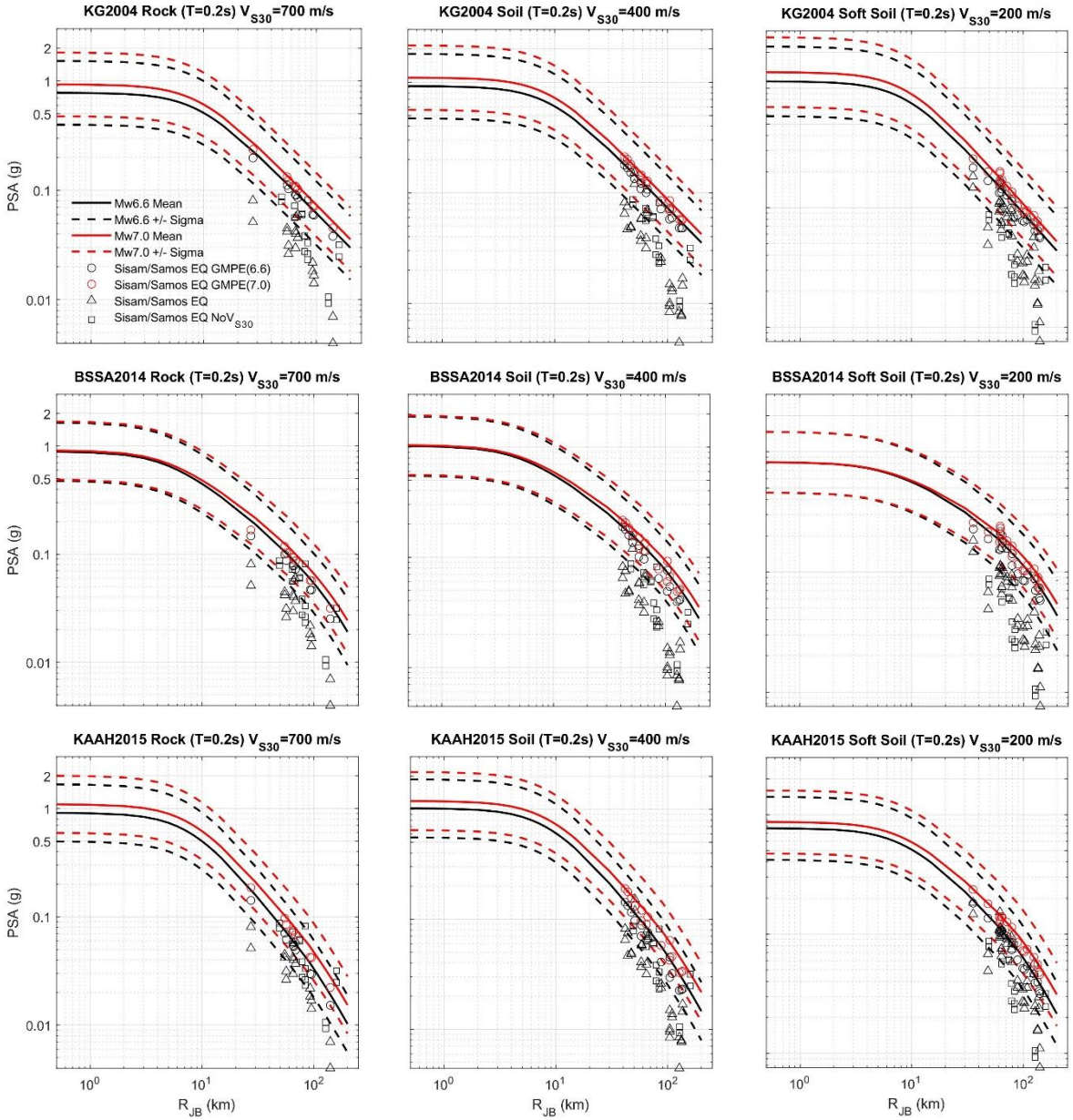

Figure 7. SA(T = 0.2 s) predictions vs measurements among three GMMs

stations which has soil class ZA and ZB are plotted on the Rock, V_{S30}=700m/s graphs while soil class ZC is plotted on Soil V_{S30}=400m/s graphs and, ZD and ZE are plotted on Soft Soil, V_{S30}=200m/s graphs.

In **Figure 6**, the PGA estimations of KG2004, BSSA2014 and KAAH2015 ground motion models are given. The stations are also checked with assumed V_{S30} values for the mean to see the dispersion with the real V_{S30} values. All models that are given in **Figure 6**, on the rock site approximately estimate the PGA values.

In **Figure 6**, KG2004 model estimates the PGA values slightly higher and excluding the stations which has distance greater than 100 km to the epicenter staying in the $\ln(Y)_{mean} \pm (\sigma_{\ln(Y)})$ band. BSSA2014 model estimates the PGA values in the the $\ln(Y)_{mean} \pm (\sigma_{\ln(Y)})$ band excluding the stations which have distances greater than 100 km to epicenter. KAAH 2015 estimating the PGA values excluding the stations with unknown V_{S30} values at rock site and a few stations at soil and soft soil conditions. The PGA estimations given in KAAH2015 staying in the $\ln(Y)_{mean} \pm (\sigma_{\ln(Y)})$ band. In **Figure 7,** the spectral acceleration (SA) estimations at T=0.2 s are given. Both of KG2004, BSSA2014 and KAAH2015 ground motion prediction models overestimating the station spectral acceleration (SA), SA(T=0.2 s) values.

In **Figure 8,** the spectral acceleration estimations at T=1.0 s are given. Regardless of the soil class differences, all station values are under the calculated mean values for KG2004 model and mostly staying in the lower band. BSSA2014 and KAAH2015 ground motion prediction models estimating the results in a range around the mean value for rock site. In soft soil and soil site graphs, the station results for SA(T=1.0 s) under the mean values and are even lower than the $\ln(Y)_{mean} - (\sigma_{\ln(Y)})$ lower limit at the distances around 100 km and above.

4. Spectrum Comparisons

In **Figure 9**, the spectral acceleration and spectral displacement spectrums of Sisam (Samos), Kusadası, Menderes, Karşıyaka-Orman İşletmesi, Bayraklı, Bayraklı-

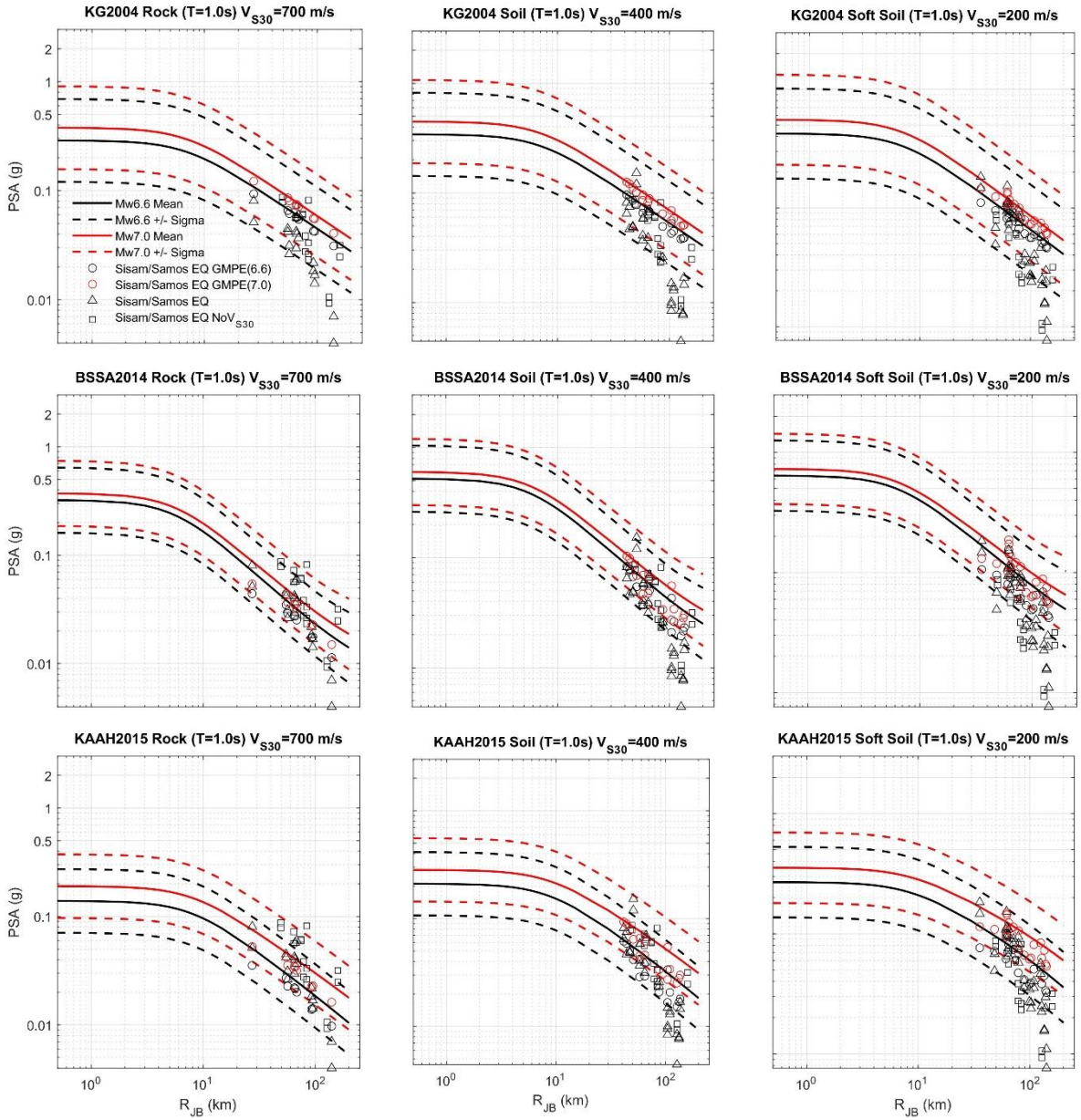

Figure 8. SA(T = 1.0 s) predictions vs measurements among three GMMs

Teknik Lise and Çeşme stations are given and acceleration-displacement response spectrum (ADRS) comparisons with TBEC (2018) are given except for the SMG1 station. The SMG1 station is not compared with the TBEC (2018) because of having no related seismic hazard analysis result for S_S and S_1 spectral acceleration coefficients.

The focus of this study is the damage distribution in the Aegean Coast of Turkey and the Turkish regulations are referred. The earthquake is a design level earthquake for Sisam, but not for İzmir and surroundings. Even it is not a design level earthquake expected for Turkey coasts, some basin affected the buildings located in Bayraklı and Karşıyaka districts of İzmir, Turkey. The damaged buildings are mostly 8 to 10 story reinforced concrete structures and constructed before 1998 which corresponds to the 1975 earthquake regulation of Turkey. There is no direct comparison of 1975 regulation with TBEC (2018) acceleration spectrum because the 1975 regulation is only referring to the design spectrum instead of elastic spectrum. Therefore, an approximate but adequate assumption is done considering the R = 6 for the RC buildings, which are the mostly damaged, and the 1975 design spectrum is multiplied with 6 to see the difference between TBEC (2018).

The ADRS graph in **Figure 9** is a good tool to check the capacity curve with earthquake demand. It can be observed that there is a basin effect in Bayraklı and Karşıyaka districts when we compare the 3513 and 3514 Bayraklı stations on soft soil and stiff soil, respectively. The amplification is almost 3 to 4 times of spectral accelerations recorded on stiff soil station and affected periods are in the 0.8 s - 1.5 s range. The spectral acceleration values are scaled to 1.0 g for SMG1 station at period of 0.5 s and the damaged structures at Sisam, mostly masonry structures [GEER (2020)], are proving this. The maximum spectral displacement is 14 cm at SMG1 station. On the Turkey side, the maximum spectral acceleration is 0.74 g at 0905-Kuşadası station and maximum spectral displacement is 17.5 cm at 3513-Bayraklı station.

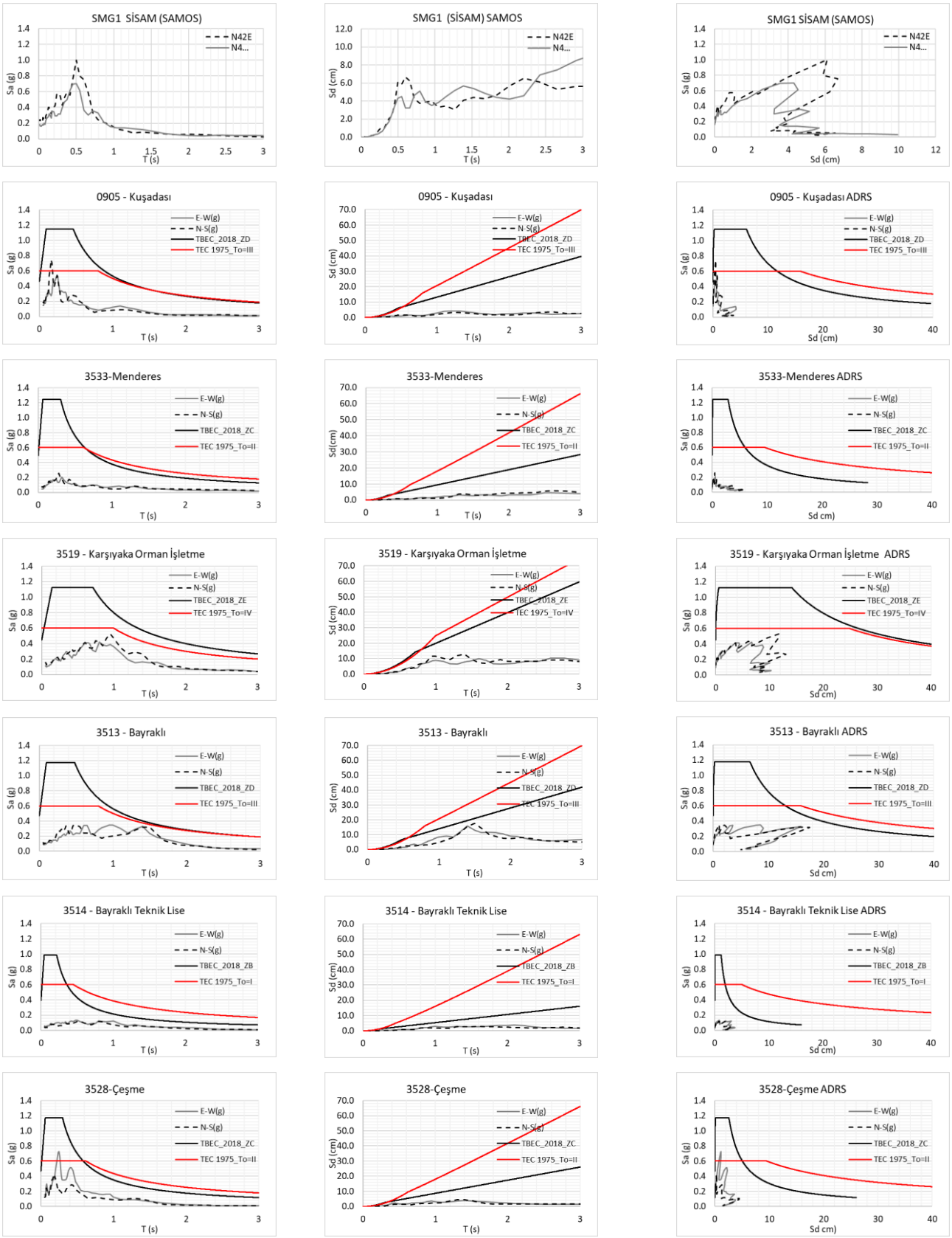

Figure 9. Spectral accelerations, spectral displacements and acceleration-displacement-response-spectrum (ADRS) plots at selected stations with the corresponding regulation-based design spectrum

5. Effects of the Earthquake on Residential Buildings

Condition assessment conducted by Ministry of Environment and Urbanization of Turkey on 145,173 buildings in İzmir shows that 90 buildings totally collapsed during and right after the earthquake, 602 (0.4%), 720 (0.5%), 6,848 (5%) and 136,913 (94%) buildings were tagged as highly, moderately, lightly damaged and no damage, respectively as shown in **Figure 10**. Results showed that the overall structural response was satisfactory. However, damage was concentrated in a certain area that indicates the soil effect played an important role on the damage of mid-raise buildings.

Significant site amplification was observed in Bayraklı district of İzmir, Turkey due to soft soil conditions and combined with the structural deficiencies of several buildings caused four complete gravity (pancake) collapses, fifty partial or sideway collapses in İzmir, Turkey. However, considering the similar typology around these buildings, which were immediately reoccupied after the earthquake, as expected based on the version of governing seismic design codes at the time of construction of the buildings, showed that heavy damages of the buildings were mainly because of the structural/material deficiencies conducted during the design and/or construction process. The objective of this paper is to provide an overview of the most common type of damage observed in Sisam earthquake.

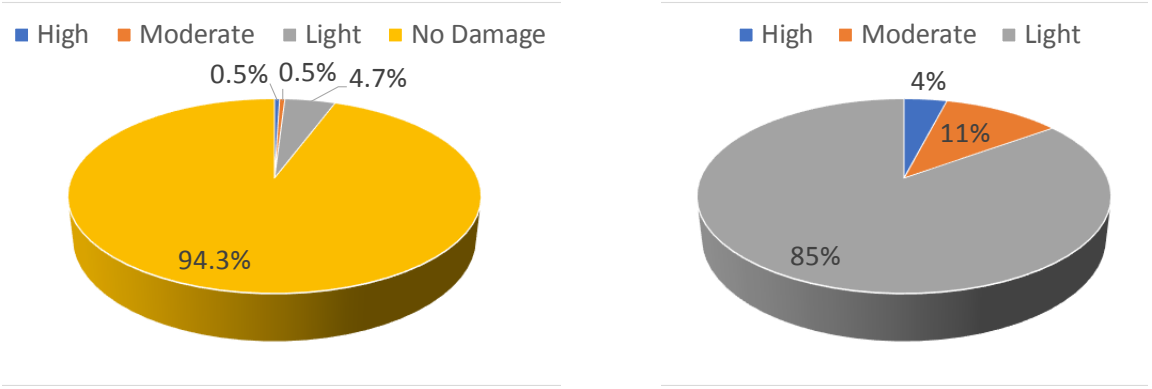

(a) (b)

Figure 10. Damage Distribution of Investigated Buildings: a) Total Damaged Buildings, b) RC Damaged Buildings

Configuration Irregularities on Structural Systems

Behavior of a multi-story building during a strong earthquake highly depends on the structural configuration. Irregularities either in horizontal or vertical configuration can lead severe damages during an earthquake. **Hata! Başvuru kaynağı bulunamadı.** shows irregular structures located in Mansuroğlu region of Bayraklı district of İzmir. Many buildings in this small area appear to have tall floor and open plaza features on the ground level. Also, shear walls which increases the lateral rigidity were not used in these buildings.

Damage of Multistory Buildings with Overhanging Floors

Close and open overhangs are widely used in Turkey for decades. Balconies, semi-balconies and extended rooms are the example of the overhangs. Previous catastrophic earthquakes in Turkey [Akansel et al. (2014)] showed that the buildings with overhangs damaged more compare to others. Even though, Turkish seismic design code allows the use of overhangs and requires them to be designed by considering the seismic loads, many application problems during the construction were reported in post-earthquake reconnaissance reports [METU (2011), GEER (2020), DAUM (2020)]. Buildings with overhang floors are also very common in İzmir, Turkey and these overhangs were the cause of the structural damages in many buildings. **Hata! Başvuru kaynağı bulunamadı.** shows the damages that occurred at the overhang locations. Columns at cantilever beam connections which intersect with overhangs are subjected to high stresses and this causes significant structural damages at these critical locations. It might be a good practice to use of reinforced concrete walls instead of columns at the cantilever beam intersections to increase the rigidity at these junctions if the overhangs are unavoidable.

Soft Stories

Large openings at the first floor have been used in the buildings for architectural purposes for many decades. Unless specific measures are taken by engineers, first floors typically have lower strength and stiffness due to lack of walls compare to the upper floors. Discontinuity in the structural system results damage concentration at the weaker or more flexible story which is commonly called soft-story mechanism. **Figure 11** shows the buildings that have suffered extensive soft-story damage/collapse. Large openings on the street side, for store windows or other purposes lead to a significantly weaker and more flexible structural frame than on the other side of the building, which has few openings, and cause topping of the building toward the street side as shown in **Figure 11**.

Torsional Irregularity

Plan geometry and rigidity distribution in plan can cause torsional irregularity. For instance, if shear walls or rigid core are located on one side of the building, flexible and rigid parts occur in the structure. Earthquake loads affect the gravity center of the structure however, the rigidity center of the structure responds to these loads for redistribution of internal forces. If the eccentricity between these two is large, torsional moment occur around the center of rigidity and causes unbalanced perimeter resistance which impose excessive forces in the farthest edge or corner columns.

Figure 12 shows examples of corner column failures. For instance, one quarter of the building was collapsed since it is located on the street corner, thus having two open sides, because of the increased axial and torsional forces at the corner columns during the main aftershock [see **Figure 12(b)**].

Figure 11. Partially collapsed buildings due to the soft story mechanism at the first floor in Bornova district in İzmir, Turkey

Figure 12. Partially Collapsed Building, Located at the Street Corner

Weak Column Strong Beam (WCSB)

Structures are allowed to be damaged at a certain level under the strong ground motions however these damages expected to be occurred at the end of the beams rather than the columns for ductile behavior in moment frames not to lead collapse. To be able to fulfill this requirement, the ultimate strength of the columns should be greater than the beams at the joints. Field observations showed that weak column strong beam (WCSB) systems are common in İzmir, Turkey might have resulted in numerous story collapses, following excessive column damage as shown in **Figure 13**.

Figure 13. Damage due to Weak Column Strong Beam (WCSB) Ratio

Short Columns

Another common type of column damage was observed when partial height nonstructural partitions were used in the buildings as shown in **Figure 14(a)**. **Figure 14(b)** and **(c)** also shows the short column effects that observed in the field. These partitions or presence of subbasement [**Figure 14(c)**] prevent the development of the column's actual flexural behavior over the height, rather allow them to deform over the free height. Even though, these short parts of the column would make it possible to resist higher lateral forces before the flexural strength of the column is reached, the shear strength of a short column is often first reached and typical non-ductile shear failures occurs.

Inadequate Seismic Joints

In last couple decades, structural engineers began to recognize that certain building shapes resulted in potentially undesirable effects, such as torsional forces and simple analysis methods may not cover these complex behaviors. To eliminate these effects, seismic joints were utilized to divide a complex shaped building into group of smaller buildings with simple shapes which can be easily analyzed. Depending of the building height and stiffness, the width of the seismic joints needs to be determined. If the width of the seismic joint was not appropriately implemented during the construction, pounding might occur when the adjacent buildings start vibration out of phase during the earthquake which causes collision amongst the adjacent building. **Figure 15** shows the structural damages due to inadequate width of the seismic joints. Previous studies [Okubo et al (2006, 2009)] showed that nonstructural partitions had positive impact on the seismic response of structures since the use of these reinforced concrete as infills, stiffens and strengthens the lateral load resistance of the structures. However, these nonstructural elements generally neglected by design engineers during the modelling process and this may cause unexpected load distribution during the seismic event. On the other hand, if only few such walls or partitions exists at the ground level, it may cause deadly damages when the ductile reinforcing details for adequate confinement is not implemented. Since the first floors were widely used as shops, department stores, banks etc., which requires large windows for exhibition, in İzmir, Turkey, fatal damages were observed when these infill walls or partitions were removed as discussed previously. **Figure 16**(a) shows in plane, shear cracks which is expected when windows locally weakens the RC column or shear wall. In other instances, it was observed that although the infills couldn't totally prevent the undesirable frame behavior, they stiffened the more flexible frames and provided energy dissipation by preventing column damages and contributed to seismic survival. On the other hand, if the infill walls poorly tied to its surrounding frame, out-of-plane collapse of infills could be observed as shown in **Figure 16**(b). Infills also played a significant role in helping the lateral strength only if the opening are not creating short column effect in surrounding columns and are not creating excessive damage in the surrounding beams such as experienced in Golcuk, Turkey (1999) The strength variation of brick and mortar of infills walls creates different failure modes and may lead to sudden drop in strength of the buildings. Similar trend was also observed in Sisam earthquake. In **Figure 16**(a), the slab discontinuity in the building results in in plane excessive infill damage (GEER (2020)).

Deficiencies due to Poor Applications

Poor quality construction materials and workmanship, non-conforming earthquake-resistant design, inadequate construction techniques and non-ductile detailing were the main reasons for extensive damages that observed in many past earthquakes in Turkey. Field observations showed that structural damages in medium buildings were mainly attributed to these effects in Sisam earthquake. The use of slender shear walls without any boundary elements, inadequate transverse reinforcement and buckling restraining crossties, contributed to widespread damage, especially when these deficiencies were coupled with soft soil conditions and irregular floor layouts. **Figure 17** shows the compression and shear failure of thin shear wall due to lack of boundary element at the basement level which lead the buckling of reinforcement after concrete crushing in the wall occurred. The structure experienced severe damage during the earthquake in the direction which the wall was very slender. The use of 90^0 bent hooks for the transverse reinforcement.

Figure 14. Short column due to presence of lower grade floors.

Figure 15. Inadequate Earthquake Joints in Bayraklı district of İzmir, Turkey

Figure 16. Damage of Infill Walls

Figure 17. Buckling of Distributed Vertical Reinforcement in Shear Walls

Detailing of reinforcement is very important for the deformation of the buildings. **Figure 18**(a) shows how widely spaced ties with 90^0 bent hooks were insufficient to contain the damaged concrete and prevent vertical bars from the buckling. Poor formwork installation was observed in many buildings in Bayrakli and Manavkuyu districts of İzmir as shown in **Figure 18**(b). Misalignment of the formwork caused cracking and structural damages in many columns and shear walls in the structure. Poor quality concrete and concrete materials were also observed in many buildings in İzmir, Turkey. This situation resulted in the concrete to exhibit an excessive porous structure **Figure 18**(c). Formation of cold joints were observed in many buildings where the cracks were occurred at these points [see **Figure 18**(b)].

Figure 20(c) shows the lap splice lengths which varies through the foundation. Inadequate lap splice length and straight ends of these laps poorly affects the overall behavior of the columns. Similar to many other buildings, improper hook detailing in stirrups was also observed as shown in **Figure 20**(b). Irregularities and deficiencies at the structures also caused problems at the overall behavior of structure as shown in **Figure 22**.

Masonry Structures

Masonry structures were observed to be less affected by the earthquake compare to the RC counterparts. The seismic loads in masonry structures are carried by the walls which has large dimensions, thus mistakes regarding the strength walls can be compensated easily compare to RC structures.

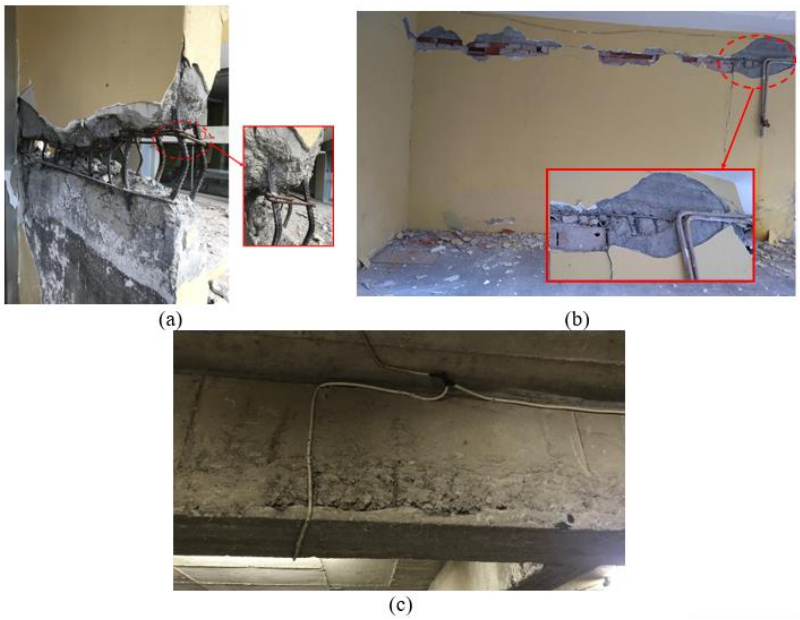

Figure 18. Defects dur to Formwork Installation, Poor Concrete Quality and Workmanship

Figure 19. Inappropriate Reinforcement Spacing and Excessive corrosion in the reinforcement

Figure 19 illustrates the reinforcement spacing which exceeds the maximum spacing requirements and inadequate confinement reinforcement. Corrosion in reinforcements took place due to insufficient concrete cover and low quality of the concrete. It was also observed that the anchorage and lap splice lengths were not properly taken care of in many severely damaged buildings as shown in **Figure 20** and **Figure 21**.

Lack of connection between the orthogonal walls in masonry structures may cause damages if these walls do not share some bricks to act together (Kaplan et al., 2008). One common place of the failure is the corners as shown in **Figure 23**. Dimensions and location of the openings in masonry structures were limited by the seismic designed codes since they reduce the area of the load bearing walls. Cracks due to large openings in the walls or windows too

close to the corners were observed at some of the university campus buildings as shown in **Figure 24** through **Figure 26**.

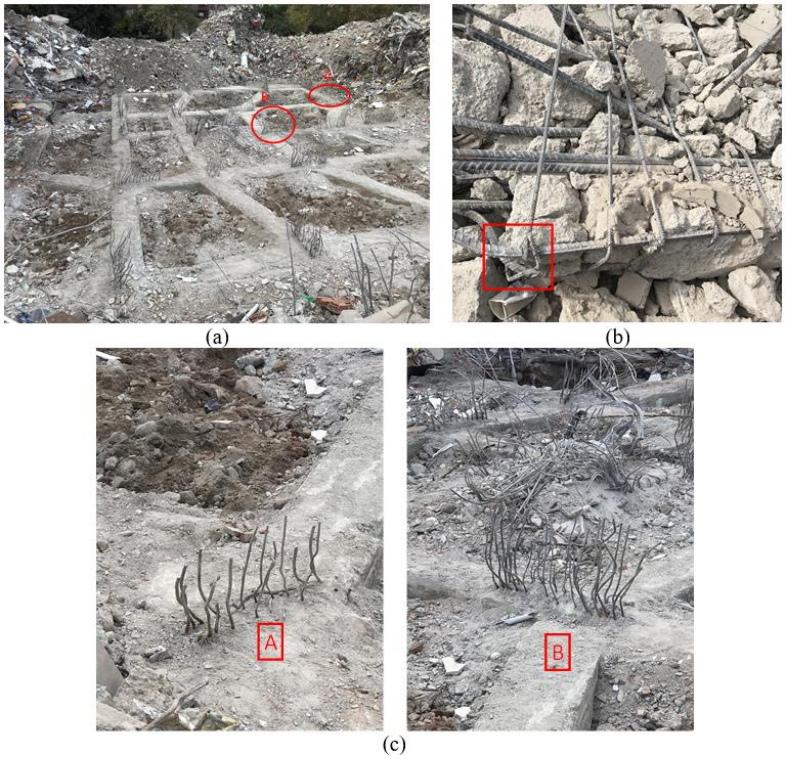

Figure 20. Inadequate lap splice length example from a collapsed building at major strike.

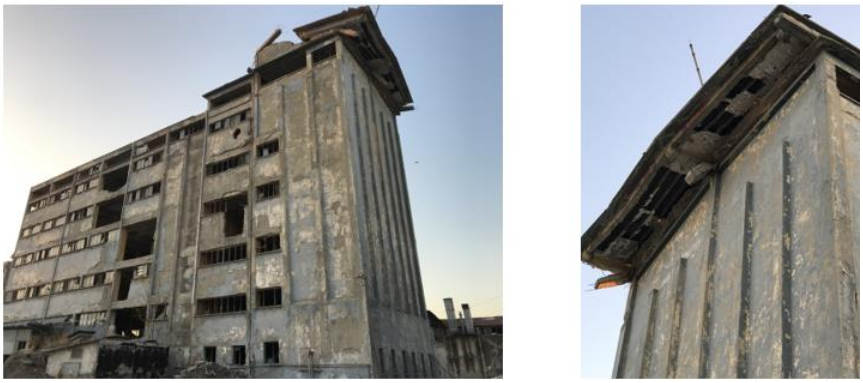

Figure 21. Damage of Abandoned Factory

Figure 22. Frame Deficiencies and Irregular Floor Layout

Figure 23. Damage at the corner of the masonry power distribution unit

Figure 24. Machine shop of Department of Agriculture at Ege University

Figure 25. School of Conservatory at Ege University

Soil supporting foundations may undergo consolidation or shear failure when subjected to excitation during an earthquake, leading to ground settlement or subsidence. The ground settlement can cause buildings to displace which may lead damages in the masonry walls as shown in **Figure 26**. The nonstructural damage was also observed. The most vulnerable top part of minaret of a mosque was collapsed while the remaining of the mosque was not even damaged. The minaret is connected to the mosque at the two story level and this creates a stiffness and boundary variation in the height and result in cracks usually at the points with abrupt cross-sectional changes which leads the minarets collapse. **Figure 27** shows the partial collapse of the minaret from the part this cross-sectional change starts.

Figure 26. School of Medicine Classrooms at Ege University

Steel Structure

In Izmir, only few buildings were constructed by using structural steel. **Figure 28**(a) shows the steel structural building with a reinforced core in the middle which was under construction when the earthquake hit the city. Before the earthquake, most of the steel frames in the buildings was completed but all the steel beam-to-column joints were visible during the earthquake. Following the earthquake, there was no connection damages on the beam to column junctions as shown in **Figure 28**(b). However, the column at the last floor which was temporarily attached to the underneath column was collapsed and caused damage to some beams at the third floor as shown in **Figure 28**(c).

good performance except few of them which have excessive non-structural damages. The main reason of having less damage in tall buildings is considered as strong foundations with ground improvement with piles. In **Figure 29**, two remarkable tall buildings, which are Folkart Towers and Mistral located in Bayraklı are given. These two towers showed good performance at main shock and have no significant structural damage. In **Figure 30**, the only damage occurred in bridges/viaducts has been showed. The viaduct is an unfinished construction more than 10 years and the fall of the girder was the result of no lateral support connection detailing.

6. Conclusions and Recommendations

The Sisam earthquake is reported with different magnitudes by different agencies and this may lead the different ground motion model results for PGA and SA values. Consistently, for all stations used in this study which has distance greater than 100 km attenuates faster than the ground motion model mean estimations and even than the lower limit. The damage distribution is mostly located on the soft soils where the basin effects shown as Bayraklı and Karşıyaka districts. The comparison of the spectrums of the soft and stiff soil of Bayraklı stations shows approximately 3-4 times of SA values of stiff soil recordings.

The rupture of the Sisam (Samos) Fault occurred in the seafloor and created a tsunami which strikes the north coasts of İzmir and economical losses occurred. The focus of the damage distribution was İzmir and its district in this study and it was observed that the affected buildings are mid-rise reinforced concrete structures located on soft soil especially. Tall buildings and bridges performed well due to high control level at design and construction stages. The main problem observed from the damaged and collapsed buildings were the improper construction and material quality, material strength decay due to inadequate maintenance, such as corrosion in the rebar, spalling of cover concrete in RC members due to deterioration, etc., and undesired structural design concerns such as strong beam and weak column frames.

Figure 27. Damage of Mosque at the Upper Part of Minaret

Tall buildings located in Bayraklı district showed


(a)


(b)


(c)

Figure 28. a) Steel Building under Construction b) Beam-to-column joints, c) Damage at the third floor beam due to collapse of a column at the construction level.

(a)

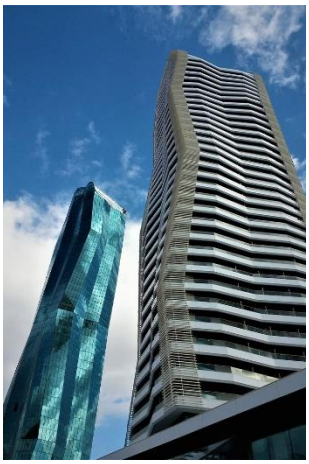
(b)

Figure 29. a) Folkart Towers b) Mistral Tower

Figure 30. a) Girder fall from unfinished bridge viaduct construction in Alsancak due to no lateral connection detailing (Photo is adapted from https://i4.hurimg.com/i/hurriyet/75/0x0/5fa6a9f00f254410e87185f2)

Acknowledgements

The author(s) wants to show their gratitude to Ozan Öğünç and Mehmet Artun Baki for their helps while gathering the station data for this study.

References

ACI Committee 318, 2019. Building Code Requirements for Structural Concrete (ACI 318-19) and Commentary, American Concrete Institute, Farmington Hill, MI

Akansel, V. H., 2007. Effect of soft story on seismic performance of reinforced concrete buildings, Ph.D. Thesis, Middle East Technical University, Ankara, Turkey.

USGS (2020), https://earthquake.usgs.gov/earthquakes/eventpage/us7000c7y0/shakemap/intensity

Kalkan, E., and Gülkan, P. (2004). Site-dependent spectra derived from ground motion records in Turkey. Earthquake Spectra, 20(4), 1111-1138.

Boore, D. M., Stewart, J. P., Seyhan, E., and Atkinson, G. M. (2014). NGA-West2 equations for predicting PGA, PGV, and 5% damped PSA for shallow crustal earthquakes. Earthquake Spectra, 30(3), 1057-1085.

Kale, Ö., Akkar, S., Ansari, A., and Hamzehloo, H. (2015). A ground- motion predictive model for Iran and Turkey for horizontal PGA, PGV, and 5% damped response spectrum: Investigation of possible regional effects. Bulletin of the Seismological Society of America, 105(2A), 963-980.

AFAD (2020a) https://deprem.afad.gov.tr/depremdokumanlari/2064

AFAD (2020b) https://www.afad.gov.tr/İzmir-seferihisar-depremi-duyuru-52-02112020---1545

AFAD (2020c) https://tadas.afad.gov.tr/

ITSAK (2020) http://www.itsak.gr/en/page/data/strong_motion/

NOA (2020) https://accelnet.gein.noa.gr/

Douglas, J. (2019). Ground motion prediction equations 1964-2018. Department of Civil and Environmental Engineering, University of Strathclyde, Glasgow, UK (available online at https://www.strath.ac.uk/staff/douglasjohndr/).

Middle East Technical University–Earthquake Engineering Research Center (METU-EERC), 2011. 23 October 2011 (Mw ¼ 7.2) Van Earthquake: Field Observations on Seismicityand Structural Damage, Report: METU/EERC 2011-04 (in Turkish), available at http://www.metu.edu.tr/sites/default/files/VanRapor_v1.6_small.pdf.

Makra, K., Rovithis, E., Riga, E., Raptakis, D. and Pitilakis, K. (2020). A note on the strong ground motions recorded in İzmir (Turkey) during the October 30th, 2020 M 7.0 Aegean Sea earthquake: The role of basin effects. A non-peer-reviewed preprint uploaded to Research Gate (November 29, 2020).

Pitilakis, K., Riga, E. and Anastasiadis, A. (2020). Towards the revision of EC8: Proposal for an alternative site classification scheme and associated intensity-dependent amplification factors. Proceedings of the 17th World Conference on Earthquake Engineering, Paper N° C002895, Sendai, Japan, September.

Gülkan, P. (2000). Building Code Enforcement Prospects: Failure of Public Policy. Chap. 15 of 1999 Kocaeli, Turkey, Earthquake Reconnaissance Report, Supplement A to Volume 16, Earthquake Spectra, December, pp. 351-367.

METU EERC (2020). 30 Ekim 2020 Mw 6.6 Sisam Adasi (İzmir Eeferihisar Açiklari) Depremi Sismik ve Yapısal Hasara İlişkin Saha Gözlemleri, Middle East Technical University, Report No: ODTÜ/DMAM 2020-03, Ankara, Turkey.

Turkish Building Earthquke Regulation (TBER) (2018). Turkish Building Earthquake Regulation, Disaster and Emergency Management Presidency, Ankara, Turkey.

Turkish Earthquake Regulation (TEC) (1975). Regulation for Buildings to Be Built in Disaster Areas, Ministry Of Public Works And Settlement, Ankara, Turkey.

ASCE/SEI (2016). Minimum design loads for buildings and other structures, ASCE7-16. American Society of Civil Engineers/Structural Engineering Institute, Reston, VA.

Earthquake Research and Application Center, DAUM (2020). 30 October 2020 Sisam (Samos) Earthquake (Mw: 6.9) Evaluation Report, Dokuz Eylül University, İzmir, Turkey. In Turkish.

Geotechnical Extreme Events Reconnaissance Association, GEER (2020). 2020 Samos Island (Agean Sea) Earthquake, Report No:GEER-069, GEER Association, doi:10.18118/G6H088.

Tan, O., Papadimitriou, E.E., Pabuçcu, Z., Karakostas, V., Yörük, A. And Leptokaropoulos, K. (2014). A detailed analysis of microseismicity in Samos and Kuşadası (Eastern Aegean Sea) areas. Acta Geophysica, Vol. 62, No. 6, pp. 1283-1309.

Ambraseys N (2009). Earthquakes in the Mediterranean and Middle East: a multidisciplinary study of seismicity up to 1900. New York, United States of America: Cambridge UniversityPress.

Havskov, J., & Ottemoller, L. (1999). SEISAN earthquake analysis software. Seismological Research Letters, 70(5), 532-534.

Boore, D. M., Joyner, W. B., and Fumal, T. E., 1997. Equations for estimating horizontal response spectra and peak acceleration from Western North American earthquakes: A summary of recent work, Seismol. Res. Lett. 68 (1), 128±153.

Bozorgnia, Y., Abrahamson, N. A., Atik, L. A., Ancheta, T. D., Atkinson, G. M., Baker, J. W., ... & Youngs, R. (2014). NGA-West2 research project. Earthquake

Spectra, 30(3), 973-987.

Ulusay, R., Tuncay, E., Sonmez, H., & Gokceoglu, C. (2004). An attenuation relationship based on Turkish strong motion data and iso-acceleration map of Turkey. Engineering Geology, 74(3-4), 265-291.

Akansel, V., Ameri, G., Askan, A., Caner, A., Erdil, B., Kale, Ö., & Okuyucu, D. (2014). The 23 October 2011 Mw 7.0 Van (Eastern Turkey) earthquake: Interpretations of recorded strong ground motions and post-earthquake conditions of nearby structures. Earthquake Spectra, 30(2), 657-682.

Okubo, K., Darama, T.H., Tamura, K., and Shiohara, H. (2006) "Lateral loading tests on precast concrete partition walls attached to structural frame with dowelbar connectors ", Proceedings of the Japan Concrete Institute, 28(3), 925- 930 (in Japanese)

Okubo, K., Shiohara, H., Darama, H., and Tamura, K. (2008) "Non-structural reinforced concrete partition walls as secondary damping devices", Proceedings of the ATC& SEI on Improving the Seismic Performance of Buildigns and Other Structures, 1034,1045.

Cetin KO, Mylonakis G, Sextos A, Stewart JP (Editors) (2020) Seismological and Engineering Effects of the M 7.0 Samos Island (Aegean Sea) Earthquake, Hellenic Association of Earthquake Engineering: Report 2020/02, Earthquake Engineering Association of Turkey, Earthquake Foundation of Turkey, Earthquake Engineering Research Institute (USA), Geotechnical Extreme Events Reconnaissance Association: Report GEER-069,

Pamuk, E., Akgun, M., Ozdag, O., Gonenc, T. (2017) 2D Soil and Engineering Seismic bed-rock modeling of eastern part pf Izmir inner bay, Turkey. J. Applied. Geophys. 137, 104-117.

Pamuk, E., Gonenc, T., Ozdag, O.C. et al. (2018a) 3D Bedrock Structure of Bornova Plain and Its Surroundings (Izmir Western, Turkey), Pure Appl. Geophys. 175, 325-340

Pamuk, E., Ozdag, O.C., Akgun, M. (2019) Soil charactization of Bornova Plain (Izmir, Turkey) and its sorrounding using a combined survey of MASW and ReMI methods and Nakamura's (HVSR) technique. Bulletin Engineering Geology and the Environment, 78(4) 3023-3035.